

Quasi-Single-Mode Fiber Transmission for Optical Communications

John D. Downie, *Member, IEEE*, Michal Mlejnek, Ioannis Roudas, William A. Wood, Aramais Zakharian, Jason E. Hurley, Snigdharaj Mishra, Fatih Yaman, Shaoliang Zhang, Ezra Ip, and Yue-Kai Huang, *Member, IEEE*

(Invited Paper)

Abstract—The transmission of a single fundamental mode in a fiber with cutoff wavelength above the transmission band is studied as a means of allowing a larger fiber effective area and reducing fiber nonlinearity. The reduction of nonlinear impairments is achieved at the expense of a potential new linear impairment in the form of multipath interference (MPI). We use a power-coupled-mode formalism to analyze the growth of MPI, and the effects of fiber and cable attributes on its magnitude and the required complexity of digital signal processing to combat the MPI. Hybrid fiber spans comprised partially of a quasi-single-mode fiber are also analyzed using a modification of the Gaussian noise model of coherent systems to predict optimal configurations, and results from transmission experiments are presented that demonstrate very high spectral efficiencies and performance surpassing that of a purely single-mode fiber system.

Index Terms—Multipath interference (MPI), optical communications, optical fiber, quasi-single-mode (QSM).

I. INTRODUCTION

THE continued strong growth of data traffic in worldwide optical communication networks drives research to enable higher spectral efficiency and system capacity over optical fiber. Higher spectral efficiency can be attained with advanced higher level modulation formats, but higher level formats with more bits/symbol generally require higher optical signal-to-noise ratio (OSNR) to get the same bit error rate (BER). One means of increasing the OSNR at the end of an optical link is to launch higher signal power, but the nonlinearity of optical fiber limits the signal power before the signal performance degrades because of deleterious nonlinear impairments [1], [2]. Digital nonlinear compensation to mitigate nonlinear effects has been the focus of much recent research in an attempt to allow higher optical channel powers and thus increase the OSNR [3]–[6]. However, such nonlinear compensation techniques are gener-

ally quite computationally expensive and only rather moderately effective to date. However, a passive means of allowing higher launch powers and OSNR values is through the use of optical fiber with lower nonlinear susceptibility. The two primary optical fiber attributes that govern nonlinear tolerance are the nonlinear index of refraction n_2 , and the fiber effective area A_{eff} . The nonlinear index is a material property and is generally lowest for silica core fibers [7]. The fiber A_{eff} is a function of the fiber index profile design, and larger A_{eff} lowers the light intensity in the core and increases the nonlinear tolerance. The largest A_{eff} of commercially available optical fibers is currently about $150 \mu\text{m}^2$ [8]–[10]. It becomes difficult to design single-mode fibers with effective areas larger than that due to competing considerations of bend loss, which tends to increase with effective area. One potential pathway to larger A_{eff} while not compromising bend loss performance is to relax the requirement of pure single-mode propagation in the fiber by increasing the cable cutoff wavelength above the transmission band, and we examine some of the issues and implications associated with this approach here.

In this paper, we first briefly motivate the use of optical fiber with larger effective area by estimating the Q and reach improvements afforded. We then review a power coupled mode model of MPI generation in fiber used for quasi-single-mode transmission, including the dependence on span length, intra-span splices, the complexity of MPI compensation digital signal processing (DSP), and differences between potential terrestrial and submarine deployments. Then we analyze coherent system performance in QSM fiber transmission in the context of the Gaussian noise model, with a focus on finding optimal hybrid fiber span configurations to maximize overall performance. Finally, we present experimental results demonstrating very high spectral efficiency trans-oceanic transmission with hybrid fiber spans including QSM fiber.

II. FIBER FIGURE OF MERIT AND SYSTEM PERFORMANCE

Almost all new long-haul terrestrial and submarine systems deployed now use coherent transmission at 100 Gb/s or higher and no optical dispersion compensation within the optical link. All chromatic dispersion compensation is done digitally in the coherent receiver, transmitter, or split between the two terminals. The performance of an optical link can then be characterized in terms of the effective OSNR (OSNR_{eff}) which takes into account the noise from amplifiers as well as from nonlinearity that

Manuscript received July 29, 2016; revised October 6, 2016; accepted October 10, 2016.

J. D. Downie, M. Mlejnek, W. A. Wood, A. Zakharian, J. E. Hurley, and S. Mishra are with Corning, Inc., Corning, NY 14831 USA (e-mail: downiejd@corning.com; mlejnek@corning.com; woodwa@corning.com; zakhariaar@corning.com; hurleyje@corning.com; mishrask@corning.com).

I. Roudas was with Corning, Inc., Corning, NY 14831 USA. He is now with Montana State University Bozeman, MT 59717 USA (e-mail: ioannis.roudas@montana.edu).

F. Yaman, S. Zhang, E. Ip, and Y.-K. Huang are with NEC Laboratories America, Inc., Princeton, NJ 08540 USA (e-mail: fyaman@nec-labs.com; szhang@nec-labs.com; ezra.ip@nec-labs.com; kai@nec-labs.com).

Color versions of one or more of the figures in this paper are available online at <http://ieeexplore.ieee.org>.

Digital Object Identifier 10.1109/JSTQE.2016.2617208

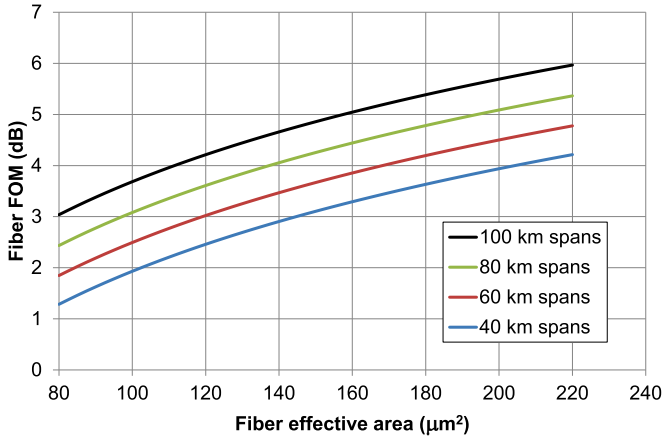


Fig. 1. Fiber FOM vs. A_{eff} . Attenuation is 0.153 dB/km. Reference fiber $A_{\text{eff}} = 80 \mu\text{m}^2$ and attenuation = 0.2 dB/km.

can be modeled as being Gaussian in nature [11], [12]. In terms of the parameters of the optical fiber in a link, the important quantities are the attenuation and nonlinear tolerance, governed by n_2 and A_{eff} . Based on the formalism of the Gaussian noise model, Nyquist WDM transmission, and OSNR_{eff} , a generalized fiber figure of merit (FOM) has been derived to quantitatively evaluate the performance of optical fibers with different characteristics [13]. Here, we employ a modified version of the fiber FOM defined relative to a reference fiber as a means of evaluating relative performance advantages [9], [14], [15]. The FOM is given in Eq. (1) and assumes nominally equivalent chromatic dispersion values for all fibers and equal amplifier noise figures. It also ignores differences in splice losses and assumes that the optimal channel launch power into the spans is used for each fiber.

$$FOM \text{ (dB)} = \frac{2}{3} \left(10 \log \left[\frac{A_{\text{eff}} \cdot n_{2, \text{ref}}}{A_{\text{eff, ref}} \cdot n_2} \right] - [\alpha_{\text{dB}} - \alpha_{\text{ref, dB}}] \cdot L \right) - \frac{1}{3} \left(10 \log \left[\frac{L_{\text{eff}}}{L_{\text{eff, ref}}} \right] \right) \quad (1)$$

In Eq. (1), L is the length of a span in a repeated system considered, and L_{eff} is the nonlinear effective length given approximately by $1/\alpha$, where α is the fiber attenuation in linear units of km^{-1} . The terms with “ref” in the subscript refer to the reference fiber. As defined here, the fiber FOM represents the difference in Q-factor, or $20\log(Q)$, between the fiber under evaluation and the reference fiber at a given transmission distance. While the FOM in general is highly dependent on both attenuation and A_{eff} , we focus on the impact of A_{eff} here since the goal of QSM fiber transmission is to allow larger A_{eff} for the fundamental mode. In Fig. 1, the fiber FOM is given as a function of effective area for span lengths ranging from 40 km to 100 km. The constant fiber attenuation is 0.153 dB/km.

While the absolute FOM value depends on span length L , it is clear that the increase or change in FOM for any A_{eff} relative to another A_{eff} is the same for all span lengths. This is also true for any fiber attenuation. For example, a fiber with $A_{\text{eff}} = 150 \mu\text{m}^2$ has a FOM advantage of almost 1.2 dB with respect to a fiber with $A_{\text{eff}} = 100 \mu\text{m}^2$, regardless of span length or



Fig. 2. Nominal span construction of a QSM fiber system.

attenuation. This corresponds to a reach advantage of about 32%. Similarly, if the fiber effective area is increased to $200 \mu\text{m}^2$, the FOM increases another 0.8 dB with additional reach increase of $\sim 20\%$. If we can increase the effective area even further to $220 \mu\text{m}^2$, then the reach relative to $A_{\text{eff}} = 150 \mu\text{m}^2$ moves to about 29%. This potential for reach increases of approximately 20–30% relative to the best currently available single-mode fiber [9] motivates the investigation into QSM fiber transmission.

III. MODELING OF QSM TRANSMISSION AND MPI

A. Model of Distributed Mode Coupling

As mentioned earlier, QSM transmission is the transmission of a signal on the fundamental LP_{01} mode of a fiber whose cutoff wavelength is at least above the lower edge of the transmission band, and likely above the whole transmission band. Thus the fiber supports a possibly leaky higher order mode, assumed to be the LP_{11} mode. The increased cutoff is allowed in order to maintain reasonable bend loss performance for a larger effective area than can be achieved with a purely single-mode fiber. The basic span model of a QSM fiber system is illustrated in Fig. 2, showing that the output of an optical amplifier is transmitted into a single-mode fiber jumper that is spliced directly to the QSM fiber with center launch. At the end of the span, the QSM fiber is again spliced back to a single-mode fiber jumper before the next amplifier. Thus we assume that only the fundamental mode is launched into each span and only the fundamental mode is captured at the end of each span.

We have developed a phenomenological model to describe propagation and the level of MPI generated by distributed mode coupling for quasi-single-mode transmission based on power coupled mode theory [16]. The model assumes launch into the LP_{01} mode of a fiber that nominally supports two spatial modes. During propagation in the fiber, optical power may couple back and forth between the fundamental and higher order modes in a continuous fashion, governed by an average power coupling strength κ (km^{-1}). At distance z in a fiber span, the optical power in the LP_{01} and LP_{11} modes can be written as follows, assuming initial conditions $P_{01}(0) = 1$, and $P_{11}(0) = 0$:

$$P_{01}(z) = \frac{1}{\delta} \left[\delta \cosh \left(\frac{\delta z}{2} \right) + \Delta\alpha \sinh \left(\frac{\delta z}{2} \right) \right] e^{-(\kappa+\alpha)z} \quad (2)$$

and

$$P_{11}(z) = \frac{2\kappa}{\delta} \sinh \left(\frac{\delta z}{2} \right) e^{-(\kappa+\alpha)z} \quad (3)$$

where $\delta \equiv \sqrt{\Delta\alpha^2 + 4\kappa^2}$, $\Delta\alpha = \alpha_{11} - \alpha_{01}$ is the differential mode attenuation (DMA) in linear units, and $\alpha = (\alpha_{11} + \alpha_{01})/2$ is the average attenuation. Employing the commonly used definition of MPI as the ratio of the total crosstalk power to the average signal power, we find the MPI generated

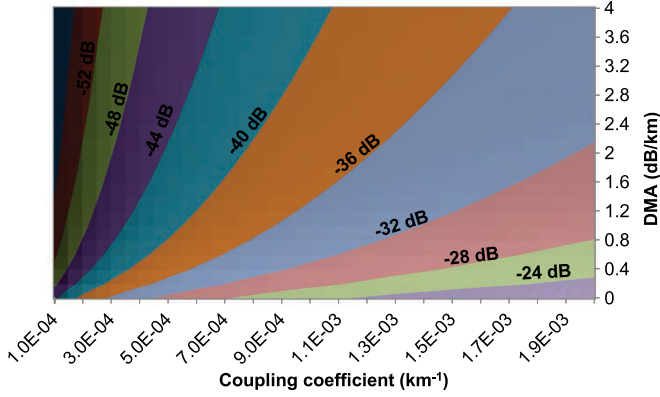


Fig. 3. Example of MPI from distributed mode coupling during propagation in QSM fiber transmission over 80 km span.

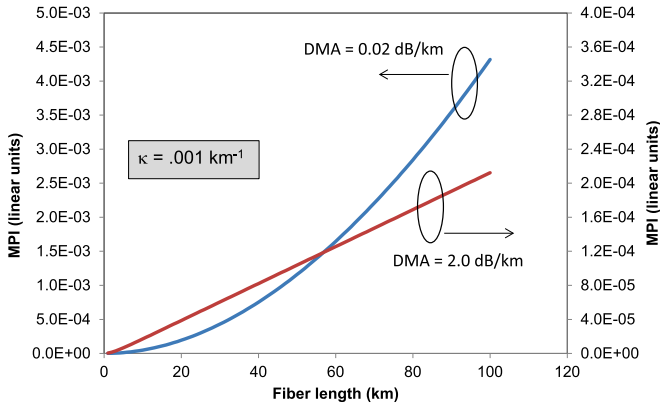


Fig. 4. Growth dependence of MPI with distance in a span for two different values of DMA.

during propagation in a single span of QSM fiber transmission can be written as [16], [17]

$$\text{MPI}(z) = \frac{(\Delta\alpha \cdot z - 1 + e^{-\Delta\alpha \cdot z})}{\Delta\alpha^2} \kappa^2 \quad (4)$$

An example of calculated MPI at the end of an 80 km span as a function of coupling strength and DMA is shown in Fig. 3. To minimize MPI generated during propagation, we wish to minimize the coupling strength and maximize the DMA. These are parameters that are dependent not only on the fiber design, but also the cabling and deployment conditions.

Examination of Eq. (4) shows that the dependence of MPI on the distributed mode coupling coefficient κ goes as κ^2 . This is because each of the crosstalk terms that build up result from two coupling events, first from LP_{01} to LP_{11} , and then back from LP_{11} to LP_{01} . On the other hand, the dependence of MPI as a function of transmission distance z varies with DMA. We can easily show that for small DMA (close to 0 dB/km), $\text{MPI}(z)$ varies as z^2 , while for larger DMA (approximately >2 dB/km) the dependence of MPI with distance z is essentially linear [16]. This is illustrated in Fig. 4 for a 100 km span with nominal $\kappa = 0.001 \text{ km}^{-1}$. Thus not only does larger DMA decrease MPI overall, but it decreases the rate of growth with distance.

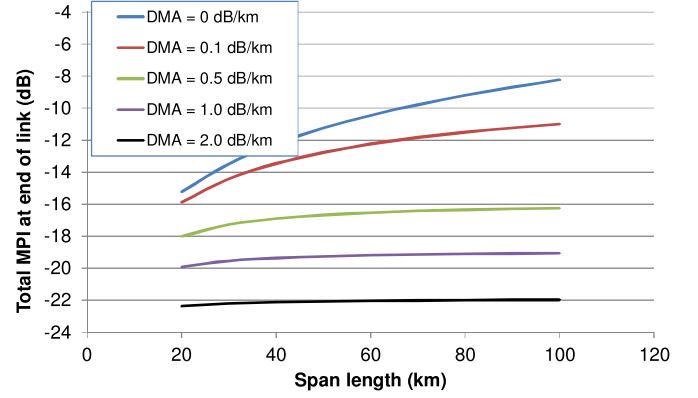


Fig. 5. Total link MPI dependence on span length for different DMA values.

As a consequence of the distance dependence of MPI growth within a span, the total MPI at the end of a multispan link may vary with span length, depending on the DMA. The total MPI will vary linearly with the number of spans since each span is independent and uncorrelated, and can thus be written as

$$\text{MPI}_{\text{link}} = 10 \log(N_{\text{spans}}) + \text{MPI}_{\text{span}} \quad (5)$$

The behavior of total link MPI as a function of span length for different DMA values is illustrated in Fig. 5 for a 3000 km link and mode coupling coefficient of 0.001 km^{-1} . For low DMA, the MPI grows quadratically with span length and it is clear that the total MPI accumulated over the link is minimized by using shorter spans. However, it appears that for DMA values ≥ 1.0 dB/km, there is no appreciable difference in link MPI with span length, at least for spans at least 30 km long. This analysis assumes that each span is comprised uniformly of the QSM fiber.

B. Inclusion of Splice Contributions to MPI

The model and results shown in the previous section were based on continuous, distributed, mode coupling that occurs during propagation in the few-mode fiber. Such mode coupling may be due to microbending loss events in the fiber. Of course, another potential source of mode coupling, and thus MPI, will be splices within the spans. For intra-span splices between pieces of the QSM fiber, small core offsets will produce loss to the fundamental mode, and coupling between the fundamental and higher order mode. To include splice loss effects in the model for MPI generation, we use numerical modeling to capture the discrete splice contributions. Taking a conservative approach, we assume that all splice loss to the fundamental mode results in the lost optical power being coupled completely into the higher order LP_{11} mode. Similarly, any optical power already in the LP_{11} mode is coupled back to the LP_{01} mode with the same coupling coefficient. The splice-generated coupling coefficient is thus given by Eq. (6), where $\alpha_{\text{splice}}(\text{dB})$ is the splice loss.

$$\varepsilon = 1 - 10^{(-\alpha_{\text{splice}}(\text{dB})/10)} \quad (6)$$

In addition to the intra-span splices between like pieces of the QSM fiber, there will also be splices at the beginning and

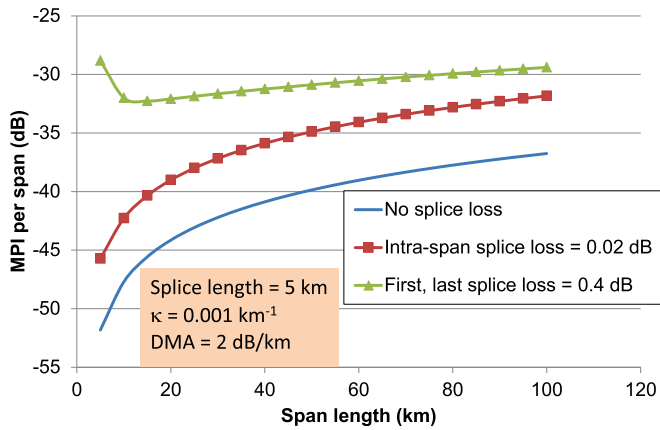


Fig. 6. MPI per span as a function of span length as calculated with numerical model including discrete mode coupling terms at splice points in addition to distributed mode coupling.

end of the span between the QSM fiber and standard single-mode fiber with significantly smaller mode field diameter, as noted earlier and illustrated in Fig. 2. Thus the first and last splices in a span will likely have significantly higher loss than the rest of the intra-span splices. In Fig. 6, we have calculated the predicted MPI as a function of span length for three cases: 1) no splice loss at all for any splices, 2) all splices having the same small 0.02 dB splice loss as might be obtained between like pieces of large mode field diameter QSM fiber, and 3) 0.02 dB splice loss for intra-span splices and 0.4 dB splice loss for the first and last splices which are between the QSM fiber and standard single-mode fiber. For these results, the distance between adjacent intra-span splices (splice length) is 5 km, the distributed mode coupling coefficient $\kappa = 0.001 \text{ km}^{-1}$, and the DMA = 2 dB/km. The inclusion of mode coupling generated at the splice points clearly has a significant effect on the total MPI. However, we do note that our assumption reflected by Eq. (6) of the relationship between the coupling and the splice loss may be overly conservative for the large splice loss assumed for the first and last splices between the fibers with dissimilar mode field diameters.

The results in Fig. 6 represent a system configuration in which each splice is made in a straight-through manner without the benefit of loops or turns of fiber on each side of the splices as might be used in splice trays. However, splice trays are commonly used in terrestrial span constructions, with several loops of fiber on each side of the splice with approximately 80 mm diameter. To assess what the impact of having such fiber loops included in a splice tray might be on the generated MPI, we first modeled the LP_{11} mode loss of several representative fabricated QSM fibers for a single 80 mm diameter circular path using a beam propagation approach and the fiber refractive index profiles. The predicted loss per turn or loop is shown in Fig. 7 as a function of the wavelength relative to the cable cutoff wavelength. The cable cutoff wavelength is defined here such that a standard cable cutoff measurement with $2 \times 80 \text{ mm}$ loops included would have a total LP_{11} mode loss of 19.34 dB [18]–[20]. For our purposes here of understanding the effect on MPI of such fiber loops in splice trays, we are interested in the

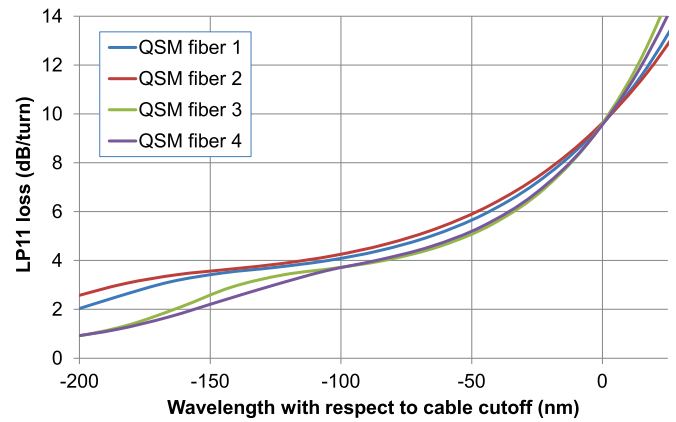


Fig. 7. LP_{11} mode loss per 80 mm diameter loop as a function of wavelength relative to cable cutoff. Results obtained from refractive index profile data of 4 fabricated QSM fibers.

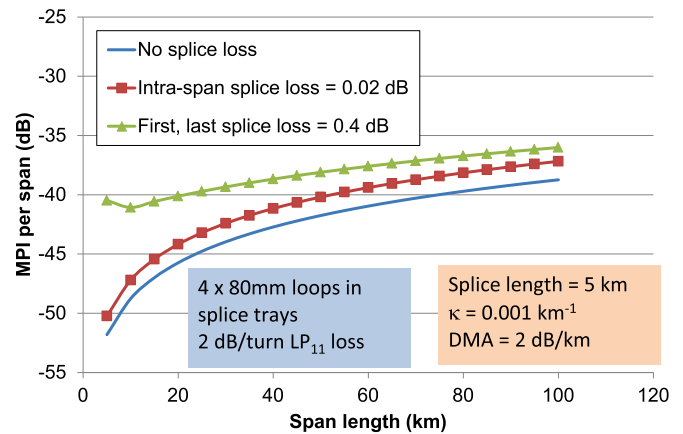


Fig. 8. MPI per span as a function of span length as calculated with numerical model including discrete mode coupling terms at splice points in addition to distributed mode coupling. Splice trays with $4 \times 80 \text{ mm}$ fiber loops on each side of the splices are also included in the model.

LP_{11} loss values below the cable cutoff. For QSM fibers with cable cutoff wavelengths in the range of 1650–1700 nm, the lowest transmission wavelength in the C-band may be approximately 120–170 nm below the cable cutoff.

For the QSM fiber data shown in Fig. 7, we can observe that this suggests that the LP_{11} loss per 80 mm diameter loop may be at least 2 dB/turn. We then used the value of 2 dB/turn loss for LP_{11} and assumed 4 fiber loops on each side of the splices to assess the impact of such a configuration on the predicted MPI as a function of span. The results for the same three cases are shown in Fig. 8. The presence of the 80 mm fiber loops in the splice trays significantly reduces the MPI generated and brings the MPI levels of the cases including realistic splice losses back much closer to the hypothetical case with zero splice losses.

The results in Figs. 6 and 8 were obtained for a splice length (distance between splices) of 5 km. It is interesting to investigate the MPI generation for different splice lengths. To do this, we considered span configurations that we believe to be reasonably representative of submarine and terrestrial systems. As noted earlier, submarine spans are constructed with straight-through

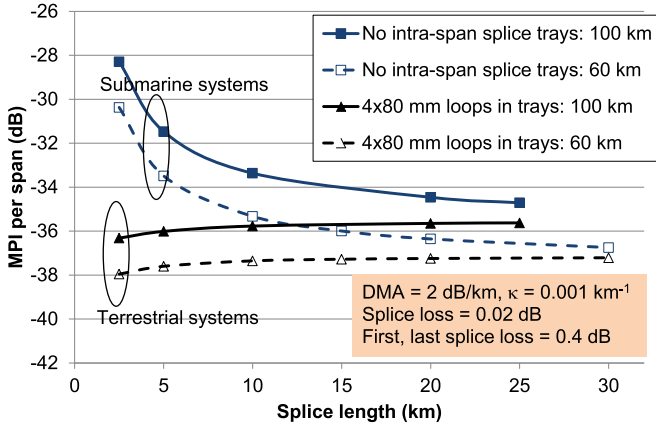


Fig. 9. MPI per span as a function of splice length for submarine and terrestrial system span configurations.

intra-span splices with fiber re-coating after splicing. Thus there are no splice trays or fiber loops for intra-span splices. However, the splices between the transmission fiber (in this case, QSM fiber) and standard single-mode fiber at the beginning and end of each span occur within the undersea repeaters and thus do have fiber loops around the splices. Thus for the submarine system model, we included 4×80 mm fiber loops surrounding the first and last splices which have higher splice losses, but no loops for any of the intra-span splices. For the terrestrial system model, we included 4×80 mm fiber loops as would be used in splice trays for every splice. Under these conditions, we evaluated the predicted MPI for both systems as a function of splice length. The results are shown in Fig. 9 for span lengths of 60 km and 100 km. In terms of minimizing MPI generation, submarine QSM fiber systems would clearly benefit from longer splice lengths within the span. On the other hand, the level of MPI generated with a terrestrial span may be effectively independent of splice length given the presence of splice trays used at every splice. In fact, the data in Fig. 9 suggest that shorter splice length may actually be slightly advantageous for terrestrial systems. This is fortunate since terrestrial spans often have splices on the order of 5 km or less, as limited by the length of cables that can be carried on trucks during deployment.

C. Effect of DMA on Maximum Effective Differential Mode Delay and MPI Compensation Complexity

As seen in earlier sections, the fiber DMA can have a strong impact on the overall level of MPI generated during propagation, as well as the rate of growth. Here we investigate the role of DMA in the required complexity of digital signal processing (DSP) to combat MPI. Compensation of MPI generated during QSM fiber transmission was first proposed [21], and then demonstrated experimentally with DSP algorithms such as decision-directed least mean squares (DD-LMS) equalization in a coherent receiver [17], [22]. In other recent related work, the DD-LMS compensation capability was studied and quantified as a function of MPI level under controlled conditions [23]. The DD-LMS equalization used in these studies involves the application of time-domain filters with symbol period spaced

taps whose weights are adaptively updated to compensate the MPI and improve the received signal quality. A key parameter of interest governing the complexity of the DSP is the number of taps required in the filters to adequately cover the range of delays of crosstalk terms relative to the signal. We address that parameter here in terms of the fiber characteristics of differential mode delay (DMD) and DMA.

We start with estimating the total crosstalk power $P_{\text{xt, total}}$ which is generated by distributed mode coupling in QSM fiber span of a length L , using a weak coupling limit approximation, $\kappa z \ll 1$, to the power coupling theory. This approximation allows us to take into consideration MPI of a portion of the launched signal that was coupled into the other mode(s) and back to the original (fundamental) mode only once; higher order terms are ignored as insignificant for weak coupling.

A signal with power P_{signal} is launched into the fundamental mode LP_{01} . At some distance z_1 some power is coupled to LP_{11} mode with the average power coupling $\kappa dz_1 P_{\text{signal}}$, where dz_1 is an incremental value of z_1 . After propagating a distance z in this mode, during which this power experiences DMA $\Delta\alpha$, a portion of the power $\kappa dz_1 P_{\text{signal}} \exp(-\Delta\alpha z)$ couples back to the LP_{01} mode at a point $z_2 = z_1 + z$ with average power coupling $\kappa dz_2 [\kappa dz_1 P_{\text{signal}} \exp(-\Delta\alpha z)]$. Integrating over all the possible occurrences of z_1 and z_2 , minding the limits of $z_1 \in [0, L]$ and $z_2 \in [z_1, L]$, we arrive in the weak coupling limit at the expression for the total crosstalk power $P_{\text{xt, total}}$ that is generated by distributed mode coupling in QSM fiber propagation:

$$P_{\text{xt, total}} = P_{\text{signal}} \cdot \kappa^2 \int_0^L (L - z) e^{-\Delta\alpha z} dz \quad (7)$$

Notice that if the integration is carried out in (7), the final result divided by P_{signal} is identical to the expression for MPI given in (4).

Consider now a QSM fiber with LP_{01} and LP_{11} modes with DMD of $\Delta\tau$ in units of (ps/km). One might think that the maximum possible absolute delay between the signal and a crosstalk term would be $L\Delta\tau$ (ps), and that the number of taps in a time domain equalizer filter should be such to accommodate this maximum possible delay. However, this overlooks the decreasing optical power in the crosstalk terms with longer LP_{11} propagation lengths, and hence longer delays relative to the signal. If the DMA $\Delta\alpha$ were 0 dB/km, the crosstalk power would decrease linearly with relative delay, and for DMA >0 dB/km, the decrease is faster than linear due to the exponential factor in Eq. (7). We can use this non-uniform crosstalk power with delay to find an effective maximum LP_{11} propagation length z_{eff} (km), and thus an effective maximum delay time T_{eff} (ps) and corresponding number of equalizer taps required for MPI compensation.

To find z_{eff} , we first determine a small fraction ε of the total crosstalk power (and thus total MPI) that we are willing to miss or ignore by using an equalizer with a number of taps that addresses $T_{\text{eff}} = z_{\text{eff}} \Delta\tau$ instead of $L\Delta\tau$. For example, if we set $\varepsilon = 0.001$, then we would find T_{eff} and z_{eff} that in principle would be able to address 99.9% of the MPI and crosstalk power. Another way to think of this is that if the actual MPI present at the receiver can be

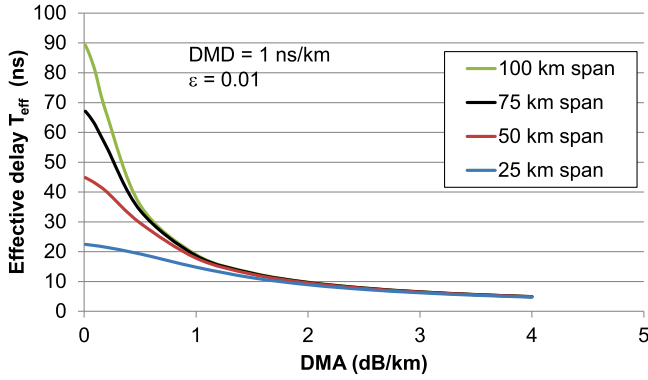


Fig. 10. Effective maximum delay of crosstalk relative to signal.

perfectly compensated with the equalizer, then the remaining MPI_{remain} after compensation would be $MPI_{\text{remain}} = \varepsilon MPI$, or $MPI_{\text{remain}} \text{ (dB)} = MPI \text{ (dB)} + 10 * \log(\varepsilon)$. Thus, if $\varepsilon = 0.001$, then $MPI_{\text{remain}} \text{ (dB)} = MPI \text{ (dB)} - 30 \text{ dB}$. Finding z_{eff} then involves solving the equation

$$\int_0^{z_{\text{eff}}} (L - z) e^{-\Delta\alpha z} dz = (1 - \varepsilon) \int_0^L (L - z) e^{-\Delta\alpha z} dz \quad (8)$$

Introducing a variable $u = \Delta\alpha(L - z_{\text{eff}}) - 1$, (8) can be reduced to

$$ue^u = [\varepsilon(\Delta\alpha L - 1) - (1 - \varepsilon)e^{-\Delta\alpha L}] e^{\Delta\alpha L - 1} \quad (9)$$

Eq. (8) has a solution in terms of the Lambert $u = W(x)$ function, which solves the equation $u \exp(u) = x$ [24]:

$$\Delta\alpha z_{\text{eff}} = \Delta\alpha L - 1 - W\left\{[\varepsilon(\Delta\alpha L - 1) - (1 - \varepsilon)e^{-\Delta\alpha L}] \times e^{\Delta\alpha L - 1}\right\} \quad (10)$$

T_{eff} is determined as $T_{\text{eff}} = z_{\text{eff}} \Delta\tau$. Fig. 10 shows calculated data for T_{eff} as a function of $\Delta\alpha$ in units of dB/km (DMA) for different QSM fiber span lengths. The DMD $\Delta\tau$ for these results is chosen as 1 ns/km and value of $\varepsilon = 0.01$.

The results in Fig. 10 illustrate that larger values of the DMA can significantly reduce the effective maximum delay T_{eff} , especially for longer QSM fiber span lengths. For the DMD and ε parameters used here, the effective maximum delay becomes effectively independent of span length for DMA values of about 2 dB/km or more. Note that for DMA = 2 dB/km, T_{eff} is less than 10% of the value for a 100 km span implied by simply using $L\Delta\tau$. The value chosen for ε strongly affects the calculated value of T_{eff} too. Fig. 11 shows the normalized number of required equalizer filter taps as a function of DMA for a span length of 75 km and different values of ε . Larger values of ε allow smaller T_{eff} and thus smaller number of equalizer taps needed to compensate for MPI generated during QSM propagation. For example, consider a DMA value of 1 dB/km. If MPI compensation is required that reduces the MPI by up to 30 dB ($\varepsilon = 0.001$), then the number of required filter taps normalized to the absolute maximum delay $L\Delta\tau$ is about 0.37. If MPI reduction by only 20 dB or 10 dB is sufficient because of relatively small MPI accumulated, then the normalized tap numbers become 0.25 and 0.125, respectively.

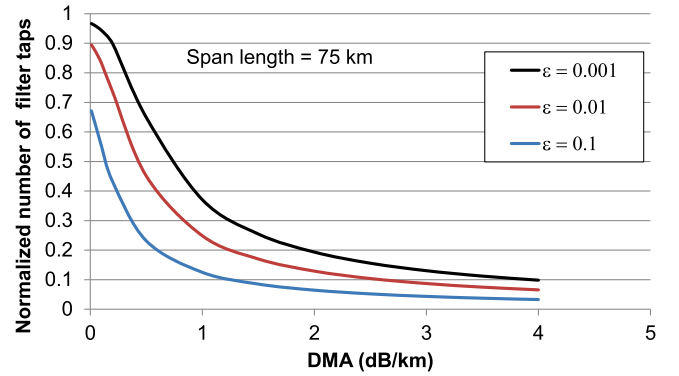


Fig. 11. Normalized number of equalizer filter taps required for different values of ε .

A previous study of MPI compensation effectiveness suggested that MPI levels of approximately -15 dB could be nearly fully compensated for PM-16QAM signals [22]. Assuming a received signal with $MPI = -15 \text{ dB}$, and using $\varepsilon = 0.01$ and the corresponding number of taps suggested by this analysis (see e.g. the red curve in Fig. 11 for 75 km spans), the residual MPI left of about -35 dB would produce an insignificant penalty after correction [25]. Lower order modulation formats such as PM-QPSK have greater tolerance to MPI [26]. Such formats may allow a larger value of ε to be used without penalty, thus further simplifying the MPI compensation DSP.

IV. MODELING HYBRID QSM AND SINGLE-MODE FIBER SPANS

In the previous section and analysis, the QSM fiber transmission system was treated as a homogeneous fiber system. However, given the competing positive and negative effects on transmission performance with QSM fiber of lower nonlinearity and MPI, respectively, it is likely that the best overall performance will be achieved with hybrid fiber span configurations [27]. A hybrid fiber span would employ the very large effective area QSM fiber at the first part of each span where the channel power is highest to minimize nonlinear impairments, and use single-mode fiber for the second part of the span to minimize the length of QSM fiber and thus reduce MPI level, delay, and DSP complexity. In this section, we derive results for optimal hybrid span configurations based on a modification of coherent system transmission using the Gaussian noise model [11], [12]. Our analysis can be applied to predict the optimal ratio of QSM to single-mode fiber lengths in a span given the relevant parameters of both fibers and the span length.

A. Nonlinear Noise in Coherent Optical Communications Systems With Hybrid Fiber Spans

Here we present an analytical model that can be used for the performance evaluation of coherent optical communication systems with hybrid fiber spans. The nonlinear distortion arising from the propagation of the signal through hybrid fiber spans is represented as an additive, zero-mean, complex Gaussian noise.

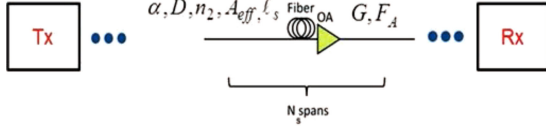


Fig. 12. Representative system without in-line chromatic dispersion compensation. A single fiber type per span is depicted for simplicity.

An analytical expression for the variance of the nonlinear noise is derived based on the formalism by Poggiolini *et al.* [11], [12].

Consider a representative coherent optical communication system without in-line chromatic dispersion compensation, as illustrated in Fig. 12. The transmission link of total length L is composed of a concatenation of N_S identical spans. In the case of coherent optical communication systems with a single fiber type per span, the optical fiber of each span has length l_S , an effective area A_{eff} , a nonlinear index coefficient n_2 , a chromatic dispersion parameter D , and an attenuation coefficient α . The optical fiber is followed by an optical amplifier of gain equal to the span loss $G = \exp(\alpha l_S)$, and noise figure F_A . In the case of coherent optical communication systems with a two fiber types per fiber span (a hybrid fiber span), the optical fiber lengths in each span are l_{S1} and l_{S2} , respectively, and their effective areas are $A_{\text{eff},1}$ and $A_{\text{eff},2}$, respectively. The corresponding nonlinear fiber coefficient γ_k of each fiber type for $k = 1, 2$ is

$$\gamma_k = \frac{2\pi n_2}{\lambda A_{\text{eff},k}}. \quad (11)$$

We assume that P is the total average launch power per channel (in both polarizations) and R_S is the symbol rate. The ideal Nyquist WDM signal is a superposition of $N_{\text{ch}} = 2M + 1$ WDM channels with spacing $\Delta f = R_S$. We evaluate the performance of the center WDM channel at wavelength λ .

The effective optical signal-to-noise ratio (OSNR_{eff}) can be well described by the analytical relationship

$$\text{OSNR}_{\text{eff}} = \frac{P}{\tilde{a} + \tilde{\beta}P + \tilde{\gamma}P^3}, \quad (12)$$

where P is the total average launch power per channel (in both polarizations), \tilde{a} is the ASE noise variance, $\tilde{\beta}P$ is the crosstalk variance due to MPI, and $\tilde{\gamma}P^3$ is the nonlinear noise variance. Explicit expressions for the coefficients \tilde{a} and $\tilde{\beta}$ as a function of the system parameters are given in [16]. Generalizing the formalism of [11], [12], the nonlinear noise coefficient $\tilde{\gamma}$ is given by the expression

$$\tilde{\gamma} = 8 \left(\frac{2}{3} \right)^3 N_S \frac{f_w^2}{\alpha^2 R_S^3} \eta_{NL} \Delta\nu_{\text{res}} \quad (13)$$

where $\Delta\nu_{\text{res}}$ is the resolution bandwidth for the measurement of the ASE noise from the optical amplifiers. In (13), we defined the four-wave mixing (FWM) efficiency as

$$\eta_{NL} = \int_0^{B_0^2/4f_w^2} \ln \left(\frac{B_0^2}{4f_w^2 t} \right) \frac{f(t) dt}{1+t^2} \quad (14)$$

where $B_0 = N_{\text{ch}} R_S$ and f_w denotes the walk-off bandwidth [28].

$$f_w = \frac{1}{2\pi} \sqrt{\frac{\alpha}{|\beta_2|}} \quad (15)$$

β_2 is the group velocity dispersion parameter and the auxiliary function $f(t)$ in the integrand of (12) is given by the following in which we assume the attenuation α of the fundamental mode LP_{01} is the same in both fiber types.

$$\begin{aligned} f(t) = & \gamma_1^2 - 2\gamma_2\gamma_1 e^{-\alpha l_S} \cos(\alpha l_S t) + \gamma_2^2 e^{-2\alpha l_S} \\ & + (\gamma_1 - \gamma_2)^2 e^{-2\alpha l_{S1}} - 2(\gamma_1 - \gamma_2) e^{-\alpha l_{S1}} \\ & \times [\gamma_1 \cos(\alpha l_{S1} t) - \gamma_2 e^{-\alpha l_S} \cos(\alpha l_{S2} t)] \end{aligned} \quad (16)$$

B. Model Results for Optimal Hybrid Span Configurations

As examples of the results obtained by application of the modified Gaussian noise model to hybrid QSM/single-mode fiber spans, we consider a system with hybrid fiber spans composed of QSM fiber and a large effective area single-mode fiber (designated SM fiber), neglecting the splice losses. We assume an ideal Nyquist WDM signal composed of 16 wavelength channels, each carrying a 32 GBd PDM-16QAM signal. The QSM fiber has effective area $A_{\text{eff},1} = 220 \mu\text{m}^2$, mode coupling coefficient $\kappa = 10^{-3} \text{ km}^{-1}$, DMA $\Delta\alpha = 2 \text{ dB/km}$ (unless otherwise stated), and combined attenuation coefficient and excess loss coefficient of 0.155 dB/km. The large effective area single-mode fiber has an effective area $A_{\text{eff},2} = 150 \mu\text{m}^2$ and attenuation coefficient of 0.155 dB/km. The resulting nonlinear coefficients are $\gamma_1 = 0.43 \text{ W}^{-1} \text{ km}^{-1}$ and $\gamma_2 = 0.57 \text{ W}^{-1} \text{ km}^{-1}$, respectively. The GVD parameter β_2 is same for both fiber types at $26.6 \text{ ps}^2/\text{km}$. The noise figure of the optical amplifiers is $F_A = 5 \text{ dB}$. The total link length is 2000 km.

Fig. 13 shows plots of the Q-factor as a function of channel launch power for a coherent optical system with 100 km spans for three span configurations of the FMF fiber and the single-mode fiber. We can distinguish two extreme cases, namely (a) with no MPI equalization and (b) with full MPI equalization. The case with no MPI equalization is shown in Fig. 13(a). Using only the single-mode fiber in each span yields an optimum Q-factor of 7.2 dB, at a launch power of 0 dBm. A better configuration is to use about 25 km of FMF fiber in the beginning of each span, followed by 75 km of the single-mode fiber at the end of each span. This fiber combination yields a slightly higher optimum Q-factor (7.6 dB), occurring at a slightly higher launch power (0.8 dBm). Using only FMF per span decreases the system performance because of the uncompensated MPI: the optimum Q-factor is 6.9 dB at a launch power of 1 dBm. On the other hand, with full MPI equalization (Fig. 13(b)) the results are quite different. Using only FMF per span is clearly the best span configuration yielding an optimum Q-factor of 8.2 dB at a launch power of 1 dBm.

Fig. 14 shows plots of the optimum Q-factor as a function of the FMF length in 100 km spans, for no MPI equalization, 50% MPI equalization, 80% MPI equalization, and with full MPI equalization. The results here all assume the optimal channel power is used in each case. As the percentage of MPI

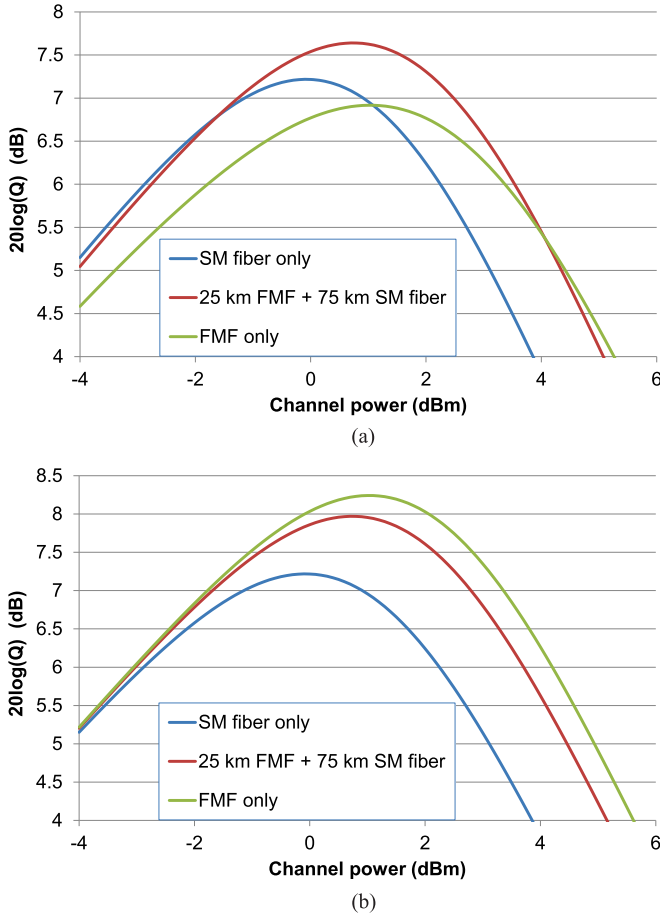


Fig. 13. Q-factor as a function of channel power for coherent optical system with 100 km spans with different fiber configurations. (a) No MPI compensation, (b) Full MPI compensation.

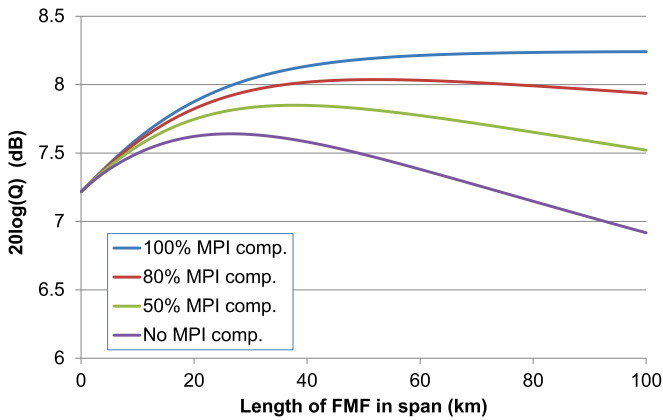


Fig. 14. Q-factor as a function of the length of the FMF used at the beginning of a 100 km span for various levels of MPI compensation performed in the coherent receiver DSP.

equalization increases, so does the optimum FMF length per span as well. For higher percentages of MPI equalization, the splitting ratio between the FMF and the SM fiber becomes significantly less critical.

The normalized optimal length of FMF in a hybrid QSM fiber span (defined as the ratio of the FMF length to the total span

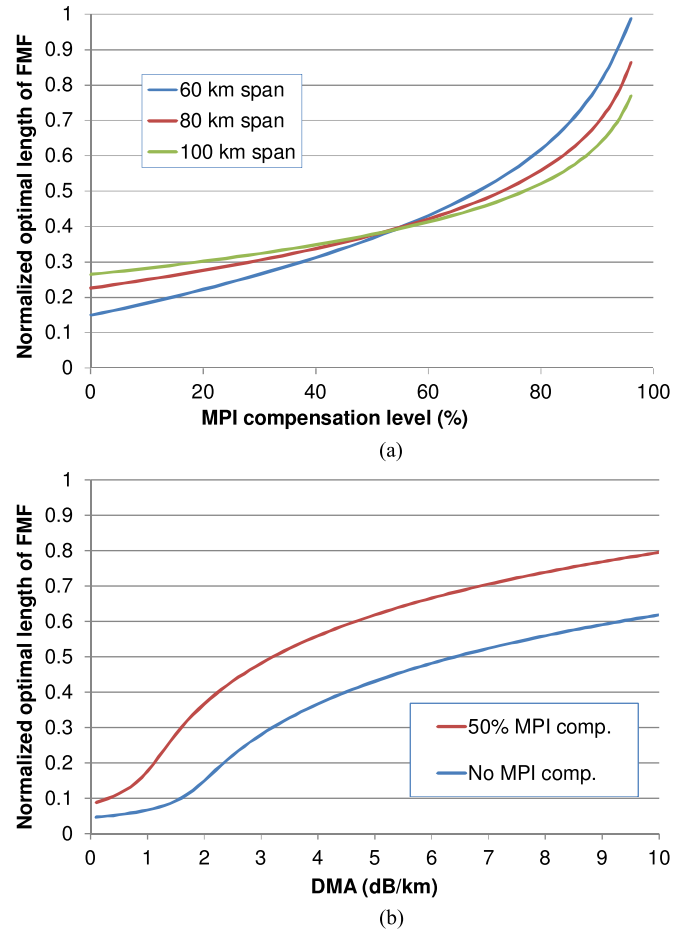


Fig. 15. (a) Normalized optimal length of FMF in a hybrid span as function of MPI compensation level for three span lengths. (b) Normalized optimal FMF length as function of DMA for a 60 km span length.

length) is given in Fig. 15(a) as a function of MPI compensation level for span lengths of 60, 80, and 100 km. As higher levels of MPI compensation are possible, the optimal ratio of FMF to the total span length increases. Similarly, in Fig. 15(b), we see that the normalized optimal FMF length also increases with DMA. The data in Fig. 15(b) is for a 60 km span, but is representative for other span lengths too.

V. TRANSMISSION EXPERIMENTS AND RESULTS

There have been a few transmission experiments in recent years focused on single-mode transmission over few-mode fibers or multimode fibers. In an early experiment, 100 Gb/s PM-QPSK transmission was demonstrated over a few-mode fiber with fundamental mode effective area of about $130 \mu\text{m}^2$, and significantly longer reach was shown in comparison to standard single-mode fiber because of the higher nonlinear tolerance [29]. No MPI impairments were observed in that experiment. 100 Gb/s PM-QPSK transmission over a $50 \mu\text{m}$ core OM3 multimode fiber (MMF) demonstrated a system reach of more than 600 km [30]. This was the longest transmission of a 100 Gb/s signal over MMF, but was ultimately limited by MPI effects. Compensation of MPI generated in QSM fiber transmission in

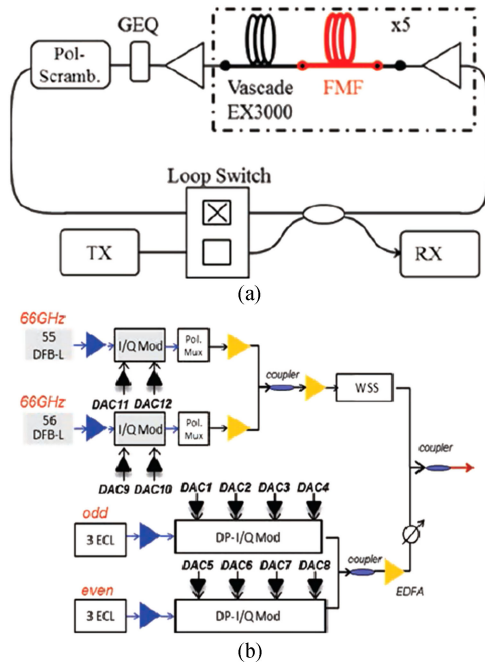


Fig. 16. (a) Re-circulating loop set-up with hybrid fiber spans. (b) Transmitter configuration with 6 tunable channels and 111 loading channels on a 33 GHz grid.

coherent receiver DSP was first demonstrated using DD-LMS equalization and showed an improvement in the received signal's Q factor and reach by more than 3 dB after compensation [22]. In this section we describe other recent transmission experiments successfully conducted with QSM fiber that demonstrated high spectral efficiency, high capacity systems over trans-oceanic distances.

In one experiment, transmission performance comparisons were made in two areas: 1) span configuration and 2) modulation format [27]. The span configurations evaluated were homogeneous fiber spans comprised of either a few-mode fiber or a purely single-mode fiber, and a hybrid span comprised of both fiber types in equal proportion. The modulation formats considered and tested were a single-carrier polarization multiplexed 16-ary quadrature amplitude modulation format (PM-16QAM) with 32 Gbaud symbol rate, and a novel multi-subcarrier format with 32 subcarriers each modulated with a 1 Gbaud symbol rate PM-16QAM signal. The two types of fiber used in the experiments were a few-mode fiber with A_{eff} of the fundamental mode of about $200 \mu\text{m}^2$ and average attenuation of 0.157 dB/km, and Vascade EX3000 fiber, a single-mode fiber with A_{eff} approximately $151 \mu\text{m}^2$ and attenuation 0.153 dB/km. The differential mode delay (DMD) of the FMF was measured to be about 1 ns/km at 1550 nm. The span lengths were approximately 102 km. In the hybrid fiber span configuration, each span was comprised of about 51 km of the FMF followed by almost the same length of the Vascade EX3000 fiber. A re-circulating loop with 5 spans as built with the hybrid fiber spans is illustrated in Fig. 16(a).

The transmitter setup used is shown in Fig. 16(b). Digital-to-analog converters (DACs) with a sampling rate of 64 GHz

generated wavelength-division multiplexed (WDM) channels on a 33 GHz grid in two groups. The first group consisted of six neighboring channels generated with tunable external cavity lasers (ECLs). These six channels were tuned together across the C-band as a group and the center channel using a narrow linewidth (<1 kHz) laser was measured. Each of the even and odd subgroups of the six tunable channels were modulated separately by 4 independent and uncorrelated streams of data for all in-phase and quadrature (I/Q) rails in both polarizations. The 111 loading channels were modulated with independent I/Q rails followed by polarization multiplexing emulators, with 15 ns relative delay between the X and Y polarizations. The tunable channels and the dummy channels are combined using a wavelength selective switch (WSS) with a 1-GHz grid resolution and a coupler. Using the DACs, either a 32 Gbaud, Nyquist-shaped single-carrier modulation (SCM) 16QAM, or a multi-subcarrier modulation (MSCM) signal of 32×1 Gbaud 16QAM subcarriers with 10 MHz guard-band was generated on each wavelength. Three different forward error correction (FEC) overheads were employed in different regions of the C-band to maximize the total capacity.

After optical filtering, each WDM channel under test was detected with a standard offline coherent receiver, using a narrow-linewidth (<1 kHz) laser as the local oscillator and a real-time 80 GSa/s sampling scope. For SCM signals, after resampling and chromatic-dispersion compensation (CDC) the signal was fed into a multi-modulus algorithm for initial convergence of polarization de-multiplexing followed by carrier phase recovery. This was followed by a second stage of equalization with symbol period spaced sampling (T -spaced) using a DD-LMS algorithm on the 32Gbaud SCM signal to mitigate MPI. For MSCM signals, after frequency offset estimation and CDC, each subcarrier was digitally filtered and processed individually in the same way as the single-carrier signal. All signal processing was performed offline.

Using the hybrid fiber span configuration with approximately 50:50 ratio of fiber lengths, we first examined the performance of the two modulation formats, especially with regard to the impact from MPI generated from the FMF sections of the spans. For the single-carrier case, the tap length of the constant modulus algorithm (CMA) equalizer was 41, and this was followed by a 1001-tap DD-LMS equalizer. This number of DD-LMS taps was found to be sufficient to maximize the MPI compensation level, and corresponded to close to ± 16 ns of addressable delay relative to the signal. For the MSCM signal, both CMA and the DD-LMS equalizers were implemented with 101 taps. The back-to-back performance of both formats was nearly identical and showed an implementation penalty relative to theory on the order of 1 dB. The measured Q-factor (based on BER data) for a central channel at 1549.7 nm is shown as a function of transmission distance in Fig. 17.

Fig. 17 shows results for both modulation formats, with and without the extra DD-LMS equalization applied. In each case, the optimal channel launch power was employed. We observe that the single-carrier PM-16QAM signal performs nearly as well as the MSCM signal up to 4060 km with the DD-LMS equalization, but is relatively degraded after that distance and

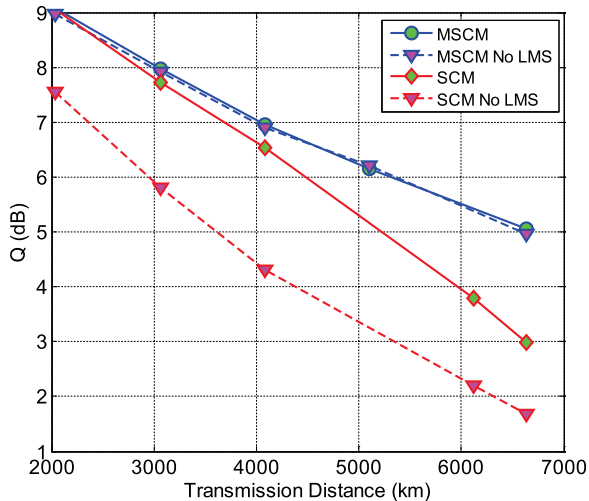


Fig. 17. Q as a function of distance for channel at 1549.7 nm for SCM and MSCM signals, with and without the DD-LMS equalization.

underperforms the MSCM signal by about 2 dB at 6600 km. The Q gain obtained from the MPI compensation was >2 dB at 4060 km. On the other hand, the CMA equalizer alone was sufficient to achieve optimal performance for the MSCM signal without the aid of the additional DD-LMS equalizer as the Q -factor results for this signal format were the same with and without DD-LMS at all distances. The multi-subcarrier format allowed a significantly smaller number of equalizer taps per sub-carrier compared to the single-carrier format. Smaller number of taps per sub-carrier allowed faster convergence of the equalizer, and better ability to follow transients in the transmission. While the total number of taps was not reduced for the MSCM signal, the effectiveness of the equalization was significantly enhanced compared to the single-carrier format. This demonstration of improved performance of a multi-subcarrier format signal in the presence of MPI from QSM fiber transmission was a key finding of the experiment. The overall spectral efficiency achieved with the MSCM signals was 6.5 b/s/Hz, and a system reach of 6600 km.

We also investigated the relative performance of the MSCM signals as a function of the span configurations, comparing the hybrid span to homogeneous fiber spans. This was done by changing the loop set-up to be comprised of 2 equal-length spans of either the hybrid fiber configuration, only Vascade EX3000 fiber, or only FMF. In Fig. 18 we show the transmission results after 10 and 20 loops circulations using the MSCM signals, and the same receiver DSP with 101-tap long CMA, and no LMS. The OSNR was varied by changing the channel launch power. The optimal channel power and OSNR was larger for the hybrid spans and all-FMF spans because of the FMF's larger A_{eff} . Some of the nonlinear tolerance advantage is negated because the MPI could not be completely compensated, as is evident in the linear regime and especially for the all-FMF span case. However, for the hybrid span case, the nonlinear improvement from the large effective area more than compensates for the penalty due to residual MPI affording 0.4 dB improvement over the all-single-mode fiber configuration. These results showing an advantage

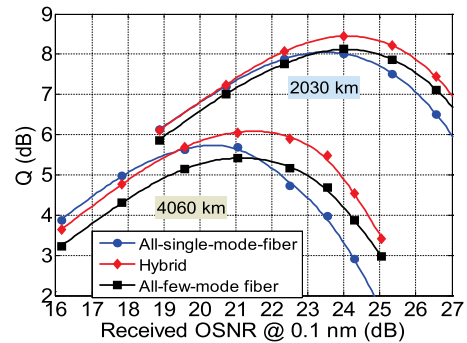


Fig. 18. Q as a function of OSNR at two distances for three fiber span configurations.

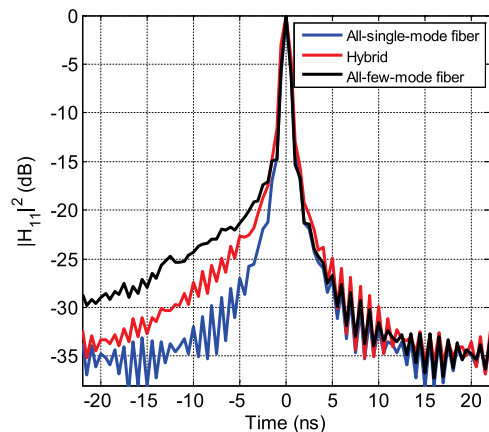


Fig. 19. CMA filter tap weights used to equalize MSCM signals after 4060 km transmission for three different fiber span configurations.

for hybrid fiber spans are in good qualitative agreement with the modeling results for hybrid spans derived in the previous section, although the various fiber parameters were not exactly the same.

Finally, another means to visualize the total MPI levels of the different span configurations is to look at the CMA tap weights. The difference in the level of total MPI suffered by the hybrid and all-FMF spans after 4060 km can be seen directly in Fig. 19 which shows the self-polarization component of the CMA equalizer filter taps used for all three span configurations after 4060 km. The leading portion of the equalizer filter is larger for the case of hybrid and all-FMF spans because of MPI since the LP_{11} mode had faster group velocity than the LP_{01} mode. It is clear that the total MPI is lower for hybrid spans compared to the all-FMF. Furthermore, inspection of the hybrid span tap weights indicates a maximum time delay of approximately 20 ns. Comparing this to the predicted t_{eff} values in Fig. 10 for roughly comparable fiber parameters suggests that the DMA of the FMF used was approximately 1 dB/km or slightly smaller. This estimate of the DMA is consistent with independent measurements of several of the FMFs used in the experiments using different techniques (not presented here), lending good support to the modeling results in Fig. 10.

Another recent demonstration of high capacity QSM transmission over a system using hybrid fiber spans increased the

spectral efficiency even higher to 8.3 b/s/Hz over a distance 6375 km [31]. There were several key enablers to this demonstration, including shorter span lengths (about 56 km), a novel modulation format (DP-64ASK) that gets closer to the Shannon limit, and higher overhead FEC. The SM fiber in the hybrid spans was the same as in the previously described experiments, but the QSM fiber here was different with slightly smaller effective area ($\sim 176\text{--}180 \mu\text{m}^2$). However, a key difference in this case was that no MPI was observed in the transmission, and thus no MPI compensation was required in the receiver DSP. The cable cutoffs of the QSM fibers used ranged from the middle of the C-band to about 1650 nm, but the LP₁₁ attenuation as deployed was sufficiently high to eliminate MPI impairments.

Finally, another potential application for QSM fiber is unrepeated system transmission, for which a hybrid span configuration again may be optimal. The short total length of QSM fiber in such a system makes MPI much less of an issue. A recent demonstration showed 401 km unrepeated transmission of PM-32QAM signals with total capacity of 20.7 Tb/s with no adverse effects from MPI [32].

REFERENCES

- [1] R. J. Essiambre, G. Kramer, P. J. Winzer, G. J. Foschini, and B. Goebel, "Capacity limits of optical fiber networks," *J. Lightw. Technol.*, vol. 28, no. 4, pp. 662–701, Feb. 15, 2010.
- [2] A. Mecozzi and R. J. Essiambre, "Nonlinear Shannon limit pseudolinear coherent systems," *J. Lightw. Technol.*, vol. 30, no. 12, pp. 2011–2024, Jun. 15, 2012.
- [3] E. Ip and J. M. Kahn, "Compensation of dispersion and nonlinear impairments using digital backpropagation," *J. Lightw. Technol.*, vol. 26, no. 20, pp. 3416–3425, Oct. 15, 2008.
- [4] E. Ip, "Nonlinear compensation using backpropagation for polarization-multiplexed transmission," *J. Lightw. Technol.*, vol. 28, no. 6, pp. 939–951, Mar. 15, 2010.
- [5] Z. Tao *et al.*, "Multiplier-free intrachannel nonlinearity compensating algorithm operating at symbol rate," *J. Lightw. Technol.*, vol. 29, no. 17, pp. 2570–2576, Sep. 1, 2011.
- [6] Y. Gao, J. C. Cartledge, A. S. Karar, and S. S.-H. Yam, "Reducing the complexity of nonlinearity pre-compensation using symmetric EDC and pulse shaping," in *Proc. 39th Eur. Exhib. Conf. Opt. Commun.*, 2013, pp. 1–3.
- [7] K. S. Kim, R. H. Stolen, W. A. Reed, and K. W. Quoi, "Measurement of the nonlinear index of silica-core and dispersion-shifted fibers," *Opt. Lett.*, vol. 19, pp. 257–259, 1994.
- [8] J. D. Downie, J. Hurley, I. Roudas, D. Pikula, and J. A. Garza-Alanis, "Unrepeated 256 Gb/s PM-16QAM transmission over up to 304 km with simple system configurations," *Opt. Express*, vol. 22, pp. 10256–10261, 2014.
- [9] S. Makovejs *et al.*, "Towards Superior transmission performance in submarine systems: Leveraging ultralow attenuation and large effective area," *J. Lightw. Technol.*, vol. 34, no. 1, pp. 114–120, Jan. 2016.
- [10] O. Levring *et al.*, "Cable and splice performance of 153 μm^2 ultra large area fiber for coherent submarine links," presented at the SubOptic Conf., Dubai, UAE, 2016, Paper TU1A.5.
- [11] P. Poggiolini, "The GN model of non-linear propagation in uncompensated coherent optical systems," *J. Lightw. Technol.*, vol. 30, no. 24, pp. 3857–3879, Dec. 2012.
- [12] P. Poggiolini *et al.*, "The GN model of fiber non-linear propagation and its applications," *J. Lightw. Technol.*, vol. 32, no. 4, pp. 694–721, Feb. 15, 2014.
- [13] V. Curri *et al.*, "Fiber figure of merit based on maximum reach," in *Proc. Opt. Fiber Commun. Conf. Expo/Nat. Fiber Opt. Eng. Conf.*, 2013, pp. 1–3.
- [14] J. D. Downie, M.-J. Li, and S. Makovejs, "Optical fibers for flexible networks and systems," *IEEE/OSA J. Opt. Commun. Netw.*, vol. 8, no. 7, pp. A1–A11, Jul. 2016.
- [15] J. D. Downie *et al.*, "Quasi-single-mode fiber transmission for submarine systems," presented at the Conf. Lasers Electro-Opt., San Jose, CA, USA, 2016, Paper TH1A.3.
- [16] M. Mlejnek, I. Roudas, J. D. Downie, N. Kaliteevskiy, and K. Koreshkov, "Coupled-mode theory of multipath interference in quasi-single mode fibers," *IEEE Photon. J.*, vol. 7, no. 1, Feb. 2015, Art. no. 7100116.
- [17] Q. Sui *et al.*, "Long-haul quasi-single-mode transmissions using few-mode fiber in presence of multi-path interference," *Opt. Express*, vol. 23, no. 3, pp. 3156–3169, 2015.
- [18] *Definitions and Test Methods for Linear, Deterministic Attributes of Single-Mode Fibre and Cable*, Recommendation ITU-T G.650.1, 2010.
- [19] F. Krahn *et al.*, "Cutoff wavelength of single-mode fibers: Definition, measurement, and length and curvature dependence," *Fiber Integr. Opt.*, vol. 8, pp. 203–215, 1989.
- [20] W. T. Anderson and T. A. Lenahan, "Length dependence of the effective cutoff wavelength in single-mode fibers," *J. Lightw. Technol.*, vol. LT-2, no. 3, pp. 238–242, Jun. 1984.
- [21] N. Bai, C. Xia, and G. Li, "Adaptive frequency-domain equalization for the transmission of the fundamental mode in a few-mode fiber," *Opt. Express*, vol. 20, pp. 24010–24017, 2012.
- [22] Q. Sui *et al.*, "256 Gb/s PM-16-QAM quasi-single-mode transmission over 2600 km using few-mode fiber with multi-path interference compensation," in *Proc. Opt. Fiber Commun. Conf.*, 2014, pp. 1–3.
- [23] J. D. Downie *et al.*, "Assessment of MPI compensation effectiveness as functions of MPI level and number of crosstalk terms for a 256 Gb/s PM-16QAM signal," presented at the Signal Process. Photon. Commun., Boston, MA, USA, Jun. 2015, Paper SpS4D.4.
- [24] R. M. Corless, G. H. Gonnet, D. E. G. Hare, D. J. Jeffrey, and D. E. Knuth, "On the Lambert W function," *Adv. Comput. Math.* vol. 5, pp. 329–359, 1996.
- [25] J. D. Downie, J. Hurley, I. Roudas, K. Koreshkov, and M. Mlejnek, "MPI measurements of quasi-single-mode fibers," in *Proc. IEEE Photon. Conf.*, Reston, VA, USA, Oct. 2015, pp. 273–274.
- [26] P. J. Winzer, A. H. Gnauck, A. Konczykowska, F. Jorge, and J.-Y. Dupuy, "Penalties from InOBand crosstalk for advanced optical modulation formats," in *Proc. Eur. Conf. Exhib. Opt. Commun.*, 2011, pp. 1–3.
- [27] F. Yaman *et al.*, "First quasi-single-mode transmission over transoceanic distance using few-mode fibers," in *Proc. Opt. Fiber Commun. Conf.*, 2015, pp. 1–3.
- [28] X. Chen and W. Shieh, "Closed-form expressions for nonlinear transmission performance of densely spaced coherent optical OFDM systems," *Opt. Express*, vol. 18, pp. 19039–19054, 2010.
- [29] F. Yaman *et al.*, "10x112Gb/s PDM-QPSK transmission over 5032 km in few-mode fibers," *Opt. Express*, vol. 18, pp. 21342–21349, 2010.
- [30] J. D. Downie *et al.*, "Transmission of 112 Gb/s PM-QPSK signals over up to 635 km of multimode optical fiber," *Opt. Express*, vol. 19, pp. B363–B369, 2011.
- [31] S. Zhang *et al.*, "Capacity-approaching transmission over 6375 km at spectral efficiency of 8.3 bits/Hz," in *Proc. Opt. Fiber Commun. Conf. Exhib.*, 2016, pp. 1–3.
- [32] Y.-K. Huang *et al.*, "20.7-Tb/s repeater-less transmission over 401.1-km using QSM fiber and XPM compensation via transmitter-side DBP," presented at the OptoElectron. Commun. Conf., Niigata, Japan, 2006, Paper PD1-4.

John D. Downie (M'08) received the B.S. degree in optics from the University of Rochester, Rochester, NY, USA, in 1983, a Certificate of Post-Graduate Study in physics from Cambridge University, Cambridge, U.K., in 1984, and the M.S. and Ph.D. degrees in electrical engineering from Stanford University, Stanford, CA, USA, in 1985 and 1989, respectively.

In 1989, he joined the National Aeronautics and Space Administration's Ames Research Center, where he was a Research Scientist and Group Leader of the Information Physics Research Group. He joined Corning, Inc., in 1999 and is a Senior Research Associate in the Science and Technology division. He has authored and coauthored more than 150 journal and conference papers to date. His current research interests include optical fibers and transmission systems for all length scales.

Dr. Downie has been a member of the Optical Society of America since 1984, including senior membership since 2007. He regularly serves as a reviewer for IEEE and OSA optics journals.

Michal Mlejnek received the B.A. and M.S. degrees in optical physics from Charles University, Prague, Czech Republic, in 1988, and the master's and Ph.D. degrees in optical sciences from the College of Optical Science, University of Arizona, Tucson, AZ, USA, in 1998.

He was a Research Associate with the Department of Mathematics and the Arizona Center for Mathematical Sciences, University of Arizona, from 1998 to 1999. He then joined Corning, Inc., Corning, NY, USA, where he has held several positions. He is currently a Senior Research Associate with the Modeling and Simulation Department, Science and Technology Division, Corning Inc. His research interests include applied mathematics, wave optics, quantum optics, and optics of materials.

Dr. Mlejnek is a member of the Optical Society of America and the Society for Industrial and Applied Mathematics.

Ioannis Roudas received the B.S. degree in physics and the M.S. degree in electronics and radio engineering from the University of Athens, Athens, Greece, in 1988 and 1990, respectively, and the M.S. and Ph.D. degrees in coherent optical communication systems from the Ecole Nationale Supérieure des Télécommunications (currently Télécom ParisTech), Paris, France, in 1991 and 1995, respectively.

During 1995–1998, he worked in the Optical Networking Research Department, Bell Communications Research (Bellcore), Red Bank, NJ, USA. During 1999–2002, he was with the Photonic Modeling and Process Engineering Department, Corning, Inc., Somerset, NJ. During 2003–2011, he was with the Department of Electrical and Computer Engineering, University of Patras, Patras, Greece, as an Associate Professor of optical communications. He has also taught as an Adjunct Professor at Columbia University, the City University of New York, and the Hellenic Open University. During 2011–2016, he was a Research Associate with the Science and Technology Division, Corning, Inc., Corning, NY, USA. Since July 2016, he has been with the Department of Electrical and Computer Engineering, Montana State University, Bozeman, MT, USA, as the Gilhousen Telecommunications Chair Professor. His current research interests include modeling and simulation of coherent optical communications systems, digital signal processing algorithms for optical transceivers, and optical interconnects. He is the author or coauthor of more than 90 papers in scientific journals and international conferences and holds five patents.

William A. Wood received the B.A. degree in physics from Colgate University, Hamilton, NY, USA, in 1984, and the master's degree in physics and the Ph.D. degree in mathematical physics from Indiana University, Bloomington, IN, USA, in 1984 and 1991, respectively.

He was a Senior Systems Engineer at Technology Service Corporation from 1992 to 1999. He then moved to Corning, Inc., Corning, NY, and has held several positions. He is currently a Research Associate with the Modeling and Simulation Department, Corning's Science and Technology Division. His research interests include applied mathematics, optical communications, and quantum optics.

Dr. Wood is a member of the American Mathematical Society.

Aramais Zakharian received the B.Sc. and M.Sc. degrees (Hons.) in physics from Yerevan State University, Yerevan, Armenia, in 1993, and the Ph.D. degree from the University of Arizona, Tucson, AZ, USA, in 2000.

He was a Postdoctoral Research Associate at the Center for Mathematical Sciences, University of Arizona, from 2000 to 2003, where he was an Assistant Research Professor at the College of Optical Sciences from 2003 to 2006. In 2007, he joined Corning, Inc., Corning, NY, USA, where he is currently a Research Associate. His research interests include development of computational methods for high-performance computing and modeling of optical and electronic components. He published more than 55 journal articles and more than 40 conference papers. He also coauthored a book titled *Numerical Time-Dependent Partial Differential Equations for Scientists and Engineers* Elsevier, 2010).

Dr. Zakharian is a Senior Member of the Optical Society of America.

Jason E. Hurley received the Associate of Applied Science degree in electronics technology from Pennsylvania College of Technology, Williamsport, PA, USA, in 1996, and the Bachelor of Science degree in electrical engineering from Alfred University, Alfred, NY, USA, in 2008. He joined the Science and Technology division, Corning, Inc., Corning, NY, in 1997. He is a Senior Scientist in the Optical Physics and Technology group, focusing on fiber characteristics to improve system performance on single mode and multimode fibers. He has coauthored more than 50 journals and conference articles and has five patents in the field of optical communications.

Snigdharaj Mishra received the B.S., M.S., and Ph.D. degrees in physics. He is a Senior Development Associate with Corning Optical Fiber, Wilmington, NC, USA. His work has included modeling and simulation, design, development, and characterization of optical fibers. He joined Corning, Inc., Corning, NY, USA, in 1999 after completing postdoctoral research works in physics at Massachusetts Institute of Technology and Max-Planck Institute, Stuttgart, Germany, and began working on submarine and terrestrial transmission fiber systems. He holds 44 U.S. patents and has coauthored more than 15 publications.

Fatih Yaman received the B.S. degrees in physics and mathematics from Koç University, Istanbul, Turkey, in 2000, and the Ph.D. degree in optical engineering from the Institute of Optics, University of Rochester, Rochester, NY, USA, in 2006.

From 2006 to 2010, he was a Postdoctoral Researcher at CREOL at the University of Central Florida. Since 2010, he has been a Research Staff Member at NEC Laboratories America, Inc., Princeton, NJ, USA. His research interests include long distance and submarine optical communication, spatial division multiplexing, nonlinear fiber optics, and fiber sensing. He is an Associate Editor of *Optics Express*.

Shaoliang Zhang received the B.Eng. degree from Beijing University of Posts and Telecommunications, Beijing, China, in 2006, and the Ph.D. degree from National University of Singapore, Singapore, in 2011. He joined NEC Laboratories America, Inc., Princeton, NJ, USA, in 2010, where his current research interests include soft-decision FEC coding, advanced modulation formats, and enhanced digital signal processing techniques for long-haul transmission.

Ezra Ip received the B.S. degree in electrical and electronics engineering from the University of Canterbury, Christchurch, New Zealand, in 2001, and the M.S. and Ph.D. degrees in electrical engineering from Stanford University, Stanford, CA, USA, in 2004 and 2008, respectively.

Since 2009, he has been a Research Staff Member at NEC Laboratories America, Inc., Princeton, NJ, USA. His research interests include space-division multiplexing, long-haul transmission, and digital signal processing techniques in coherent transmission systems.

Yue-Kai Huang (M'04) received the B.S. degree in electrical engineering and the M.S. degree in electrooptical engineering from National Taiwan University, Taipei, Taiwan, in 2000 and 2002, respectively, and the Ph.D. degree in electrical engineering from Princeton University, Princeton, NJ, USA.

He joined NEC Laboratories America, Inc., Princeton, first as an intern in 2007 and then as a Research Staff in 2008, and is currently Senior Researcher. He has published more than 100 journal and conference papers and is an inventor of 15 U.S. patents. His research interests/projects include optical superchannel transmission technologies, high-speed optical transmitter and receiver design, and spatial division multiplexing techniques for signal transmission over novel fibers.

Dr. Huang has organized workshops in ECOC and GlobeCOM and is currently a TPC member for CLEO. He serves as a Reviewer for many journals including IEEE PHOTONIC TECHNOLOGY LETTERS, JOURNAL OF LIGHTWAVE TECHNOLOGY, and *Optics Letters*.